Dispersive Shock Waves in Nonlinear Arrays

Shu Jia, Wenjie Wan, and Jason W. Fleischer

Department of Electrical Engineering, Princeton University, Princeton, New Jersey 08544, USA

(Received 27 April 2007; published 27 November 2007)

We experimentally study dispersive shock waves in nonlinear waveguide arrays. In contrast with gap solitons, the nonlinearity here pushes the propagation constant further into the transmission bands, facilitating Bloch mode coupling and energy transport. We directly observe this coupling, both within and between bands, by recording intensity in position space and power spectra in momentum space.

DOI: 10.1103/PhysRevLett.99.223901 PACS numbers: 42.65.Wi, 46.40.Cd, 47.37.+q, 47.40.−x

Dispersive shock waves are a fundamental type of nonlinear wave and appear in many hydrodynamic settings, including fluids, superfluids, plasma, and optics [1]. Their basic existence conditions are a dispersive medium with an effective pressure (e.g., repulsive interactions or defocusing nonlinearity) and a fluid or intensity background that can support undamped waves. In the ensuing dynamics, the initial wave profile steepens, with different modal components coupling to the background and walking off from each other. The result is an expanding front characterized by oscillations (rather than the monotonically-decreasing front that characterizes dissipative shock waves). Even from a discrete, or atomistic, viewpoint, such oscillatory fronts arise whenever (nonlinear) elastic motion dominates viscous or plastic flows. Examples in this case include nonlinear mass-spring systems [2–4], molecular [5] and granular [6] media, bubbly fluids [7], and dusty plasmas [8]. To date, however, these discretized studies have relied on a tight-binding approach, which minimized the unique properties of the underlying Floquet-Bloch mode structure and ignored coupling between transmission bands. Here, we consider the photonic case experimentally by observing dispersive shock waves in a nonlinear waveguide array. We show both fundamental and higher-band lattice shocks and demonstrate explicitly enhanced energy transport due to multimode coupling.

The waveguide system studied here is well-described by the nonlinear Schrödinger equation

$$i\frac{\partial\psi}{\partial z}+\frac{1}{2k_0}\nabla_\perp^2\psi+V(x)\psi+\Delta n(|\psi|^2)\psi=0 \qquad (1)$$

where ψ is the slowly-varying amplitude of the optical field, $k_0=2\pi n_0/\lambda$ is the wave number in the material, $V(x)$ is a periodic potential, and Δn is the nonlinear index change induced by the light intensity. For a medium with a Kerr response, for which most theory is done, $\Delta n=n_2k_0|\psi|^2/n_0$, where n_2 measures the strength of the nonlinearity ($n_2<0$ for defocusing). For the experiments, a $(2\times5\times10)$ mm SBN:75 ($Sr_{0.75}Ba_{0.25}Nb_2O_6$) crystal is used. In this case, the photorefractive nonlinearity $\Delta n=-(1/2)n_0^3r_{33}E_{\rm app}\bar{I}/(1+\bar{I})$, where $n_0=2.3$ is the base index of refraction, $r_{33}=1340$ pm/V is the appropriate electro-optic coefficient with respect to the applied field $E_{\rm app}$ and the crystalline axes, and the relative intensity $\bar{I}$ is the input intensity $|\psi|^2$ measured relative to a background (dark current) intensity [9,10]. A self-defocusing nonlinearity is created by applying a voltage bias of -125 V across the crystalline c-axis and taking advantage of the photorefractive screening effect. In most cases, the use of defocusing nonlinearity minimizes the difference between saturable and Kerr systems [11]. For example, results from recent homogeneous shock experiments, using a photorefractive setup identical to the one considered here, matched Kerr predictions exactly [1].

The (super)fluid interpretation of the dynamics comes from applying the Madelung transformation $\psi(x,z)=\sqrt{\rho(x,z)}\exp[iS(x,z)]$ to Eq. (1), where $\rho=|\psi|^2$ is the intensity and S is the coherent phase of the wave function [12]. Scaling $(x,z)\rightarrow k_0(x,z)$ then gives two Euler-like equations for the optical "fluid":

$$\frac{\partial\rho}{\partial z}+\nabla_\perp(\rho v)=0 \qquad (2)$$

$$\frac{\partial v}{\partial z}+v\nabla_\perp v=-\frac{n_2}{n_0}\nabla_\perp\rho-\nabla_\perp V+\frac{1}{2}\nabla_\perp\left(\frac{1}{\sqrt{\rho}}\nabla_\perp^2\sqrt{\rho}\right) \qquad (3)$$

where $v=\nabla_\perp S$ is the "fluid" velocity. Note that this definition is consistent with the eikonal intuition of the wave front normal giving the direction of energy transport, though care must be taken comparing Bloch vs Fourier momentum $\mathbf{k}$ when propagating in an array. Equation (2) states that intensity is conserved while Eq. (3) states that optical flow arises from three effective pressures: one from the repulsive (defocusing) nonlinearity, one from the external (lattice) potential, and one from diffraction. The left-hand side of Eq. (3) is a convective derivative, implying that an initial velocity (phase) profile will self-steepen as it propagates. As the wave breaks, a shock is formed. However, there is no dissipation in the system, so the wave front does not have the sharp, nearly-discontinuous profile common in viscous fluids. Instead, the velocity gradient is regularized by modal dispersion, creating a front that is characterized by oscillations (phase interference). These

dispersive shocks are typical of inertial fluids and collisionless plasma described by the Korteweg–de Vries equation [13], as suggested by the triple derivative of the diffraction term, and of superfluids described by Eq. (1). A good comparison between dispersive and dissipative shock waves can be found in Ref. [14].

The experimental setup is shown in Fig. 1. It consists of three basic parts: (1) an ordinarily-polarized pair of plane waves to optically-induce a lattice structure [15,16], (2) an extraordinarily-polarized hump-on-background profile as input [1], and (3) an imaging system to observe the light exiting the crystal. The two-stage input, formed by splitting 532 nm laser light using a Mach-Zehnder interferometer, takes advantage of the optical anisotropy of the SBN crystal: the 1D array of waveguides stays fixed during propagation, while the shock beam experiences both the fixed periodic potential and a self-defocusing nonlinearity. At the exit face of the crystal, the output is imaged into two CCD cameras, one for the direct (near-field) intensity in position (**x**) space and one for the Fourier (far-field) intensity in momentum (**k**) space.

Figure 2 shows the linear transmission spectrum and underlying Floquet-Bloch modes of the waveguide array. As is well-known, the spectrum consists of bands of allowed propagation separated by forbidden gaps, the geometry of which characterizes the diffraction/dispersion relation $\beta = k_z(k_x)$. Momentum regions with concave curvature (e.g., the odd-numbered modes in Fig. 2) experience normal diffraction, in which the wave front diverges while propagating, while regions with convex curvature experience anomalous diffraction [17]. These two regions respond differently to a given nonlinearity, with diffraction either enhanced or suppressed depending on the relative sign of the curvature. For example, lattice solitons are formed when nonlinearity exactly counteracts diffraction, e.g., self-focusing nonlinearity for modes 1 [18] and 3 [19] and self-defocusing nonlinearity for mode 2 [16] in Fig. 2. With nonlinearity present, the propagation constant no longer lies on the linear transmission curves; in the soliton cases, it is pushed into the gap, localizing the wave in the self-induced defect and isolating it from the linear modes of the array [11]. Here, we consider the opposite regime in which the propagation constant is driven farther into the transmission band, facilitating the nonlinear coupling of modes.

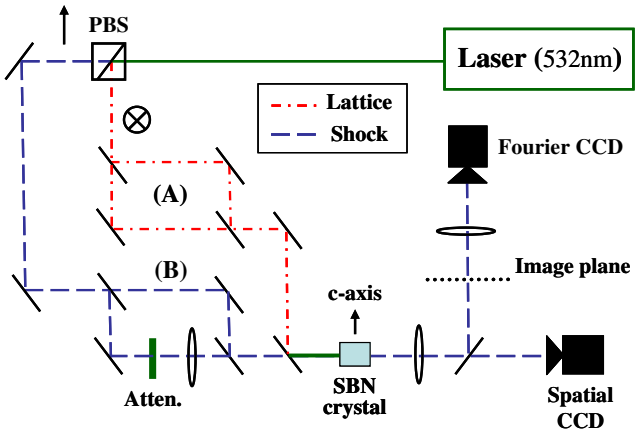

FIG. 1 (color online). Experimental setup. Light from a 532 nm laser is first split by a polarizing beam splitter. The ordinarily-polarized beam passes through a Mach-Zehnder interferometer (a) to induce a waveguide array in an SBN:75 crystal. The extraordinarily-polarized beam passes through a modified Mach-Zehnder interferometer (b) to create a Gaussian-on-background input shock profile. Light exiting the crystal is imaged into two CCD cameras, one for the intensity in position (**x**) space, one for the power spectrum in momentum (**k**) space (obtained by performing an optical Fourier transform). To excite a second-band Bloch background for a higher-band shock, the plane wave arm in (b) is blocked and the interferometer in (a) is partially polarized in the extraordinary direction.

Experimental shock waves, along with numerical simulations, are shown in Fig. 3. For reference, a dispersive shock wave in the homogeneous crystal (no induced array) is shown in Fig. 3(a). The input, not shown, consists of a Gaussian beam superimposed on a plane wave, with an intensity ratio of 10:1. As the beam is defocused, it runs into the surrounding background, creating a shock wave with an oscillating front. Dynamically, the high-intensity part acquires a nonlinear phase that the low-intensity background does not; when the two regions overlap, the phase difference causes an interference pattern. Mathematically, the front can be described in terms of a Jacobi elliptic function [20]. The inner part of the front consists of a series of dark (gray) solitons, while the outer part consists of linear, soundlike oscillations about the background. More details about such homogeneous shock waves can be found in Ref. [1].

Figure 3(c) shows the output of the same hump-on-background profile launched into a waveguide array with period $D = 30\ \mu$m. In this case, the intensity ratio of hump to background remains 10:1 while the hump-to-lattice ratio is 1:1. Compared with the homogeneous case [Fig. 3(a)], two features of the lattice shock are clearly visible: the front does not propagate as fast, and the

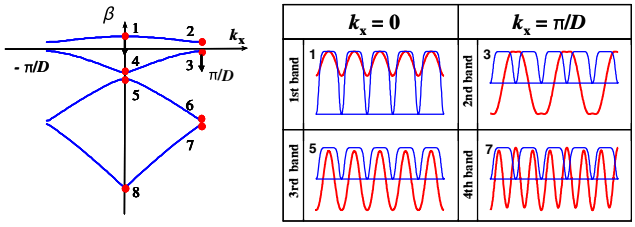

FIG. 2 (color online). Linear transmission spectrum in the reduced Brillouin zone scheme, showing key propagation constants and field profiles of representative modes. Modes numbered 1 and 3 are the initial background k-vectors, and the arrows indicate the effect of defocusing nonlinearity.

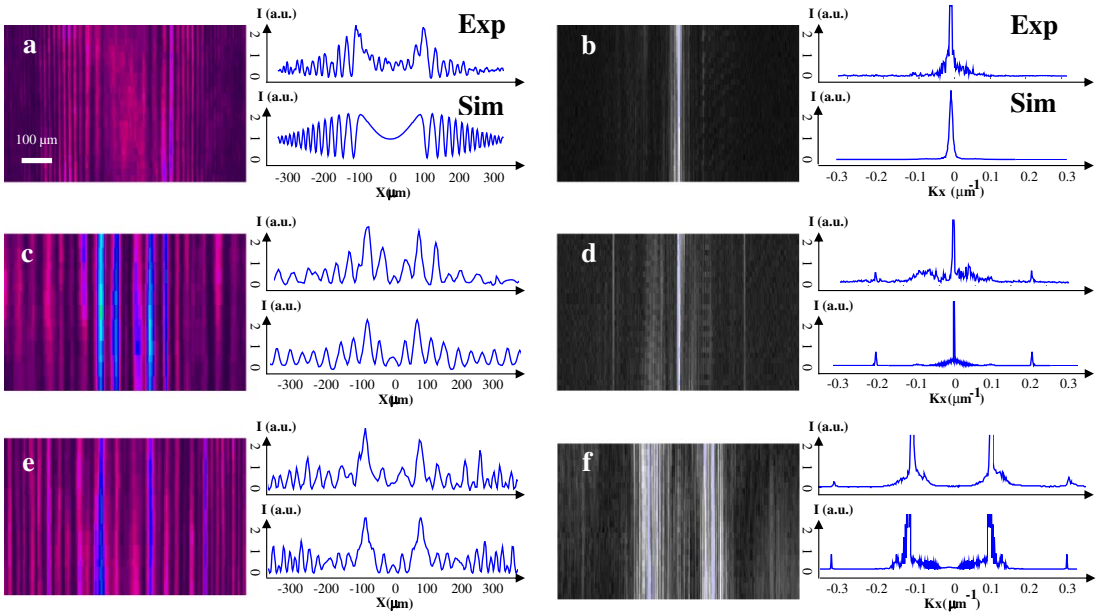

FIG. 3 (color online). Output pictures of dispersive shock waves in homogeneous and lattice systems. Left column: intensity in position (**x**) space; right column: power spectrum in momentum (**k**) space. The left side of each panel shows experimental output pictures, while the right side shows cross sections from experiment (top) and beam propagation simulation (bottom). For a Gaussian-on-background input intensity ratio of 10:1, the pictures show shock waves (a,b) in homogeneous system; (c,d) against fundamental, first-band background (modes 1 +); (e,f) against second-band, cosine background (mode 3). In (c–f), the period of the lattice is 30 μm. Note that in (f), the first Bragg peaks have been saturated to allow visualization of the less-intense, higher-order modes.

smaller-scale oscillations are lost. Both features are due to the lattice potential. In the first feature, the propagating front must overcome the periodic energy barrier as it tunnels from site to site. In the second feature, the size of the waveguide (potential well) sets the spatial scale for oscillations.

Further insight into the basic shock behavior can be obtained from the power spectrum, shown in Figs. 3(b) and 3(d). For the homogeneous shock, there is a large peak at $k = 0$, due to the plane wave background, surrounded by two broader bands: an inner one representing large-scale envelope modulations and an outer one representing the small-scale oscillations in the shock tails. For the discretized shock, the central peak remains, but two additional side peaks appear, one each at the double-Bragg angles $\pm 2k_B = \pm 2\pi/D$. The reasons for these can be seen in Fig. 4, where we propagate each of the input components separately through the nonlinear array. For the Gaussian input beam [Figs. 4(a) and 4(b)], the output intensity profile is a Gaussian $\exp[-x^2]$ modulated by the optical lattice. The corresponding k-space output consists of two separated Gaussian humps, resulting from the Fourier transform $\cos(k_B x)\exp[-x^2] \rightarrow \exp[-(k - k_B)^2/4] + \exp[-(k + k_B)^2/4]$. The nonlinear output spectrum of the plane wave input is shown in Figs. 4(c) and 4(d). As can be seen, this uniform input excites a broad spectrum of modes across the first band, with dominant peaks at $k = 0$ and $k = \pm 2k_B$. These latter peaks are a direct result of the lattice periodicity, aided by the nonlinearity pushing down the propagation constant (from mode 1 in Fig. 2 to mode 5). Note that it is mode 5 from the third band, rather than mode 4 from the second band, because of the concave curvature of the band; also, excitation of this mode sharpens the edges within the waveguides (its dipole structure is phase-shifted), rather than contributing an intensity dip in the waveguide centers. The fact that the broad output peaks at $\pm k_B$ from the Gaussian input [Fig. 4(b)] do not appear in

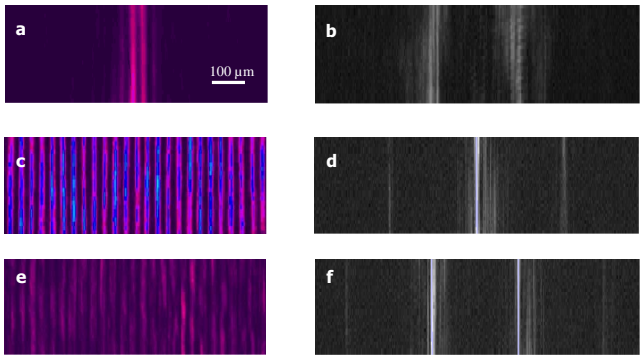

FIG. 4 (color online). Output pictures of different initial intensity profiles in optical lattices. (a,b) Bright Gaussian hump with width 15 μm, intensity ratio 1:1 to the lattice; (c,d) plane background wave, with intensity ratio 1:10 to the lattice; (e,f) cosine background wave, with intensity ratio 1:10 to the lattice. The period of the lattice is 30 μm. Left and right columns show intensity in position (**x**) space and power spectrum in momentum (**k**) space, respectively.

the discretized shock spectrum [Fig. 3(d)] means that the energy initially in the Gaussian hump has been effectively coupled to the background light.

Understanding the energy transfer in the discretized shock wave is complicated by the fact that the background plane wave is not a pure eigenmode of the underlying lattice. To consider a purer lattice shock wave, we launch the initial Gaussian input against the cosine Floquet-Bloch mode at the edge of the first Brillouin zone (mode 3 in Fig. 2). This mode is excited by partially rotating the polarization of the array beams [Fig. 1(a)] in the extraordinary direction and recalibrating the intensity ratios. The resulting shock wave is shown in Fig. 3(e). The intensity peaks occur in the same location as the previous lattice shock [Fig. 3(c)], as the intensity parameters are the same in both cases. However, there is much more intensity and higher spatial resolution in the shock tails, evidence of coupling to higher-order modes. This coupling is shown explicitly in the output power spectrum of Fig. 3(f). In this case, the two high peaks at $\pm k_B$ correspond to the initial cosine mode. The spread around these peaks shows clear coupling to other modes within the band. In contrast with the broad first-band excitation in Fig. 3(d), there is a sharp cutoff halfway through the Brillouin zone as the band curvature changes sign. As before, though, the nonlinearity couples the initial background mode to the next-higher mode modulo $2\pi/D$. These are the peaks appearing at an additional $\pm 2k_B$ in Figs. 3(f) and 4(f).

As a final note, we would like to point out analogous results possible in the temporal, rather than spatial, domain. In this case, the initial condition consists of a pulse atop a background, e.g., in an optical fiber, with new modes corresponding to new frequencies. For example, the blueshifted wavelengths produced in supercontinuum generation are dispersive [21]; if their intensity is high enough, they will experience a repulsive nonlinearity which can induce shock waves [22]. If the fiber also has a Bragg grating [23], then the pulse dynamics will follow the same lattice dynamics demonstrated here. In particular, higher-band modes will be excited, leading to new possibilities for parametric pumping, new frequency generation, and control.

In conclusion, we have studied dispersive spatial shock waves in optical waveguide arrays. Compared with the homogeneous case, new features include an effective resistance due to the lattice potential and a more complex means of energy transfer due to the underlying Floquet-Bloch modes. These modes give rise to a whole family of lattice shock waves, just as with lattice solitons. Unlike gap solitons, which are nonlinear localized modes with propagation constants (energy eigenvalues) residing inside a band gap, lattice shock waves have their propagation constants pushed farther into the transmission band. This facilitates mode coupling and energy dispersal, including and especially the excitation of higher-band modes. This was demonstrated for Gaussian input profiles defocused against first-band and second-band backgrounds, but it is clear that these are just representative examples of a much richer range of lattice shock waves. When extended to the temporal regime, for example, the dynamics suggest a method of controlling the production of new frequencies, e.g., pumping blueshifted, normally-dispersive waves in supercontinuum generation. Hence, we expect many more examples of shock-mediated photonic dynamics in the near future.

This research was supported by the NSF and AFOSR.

[1] W. Wan, S. Jia, and J. W. Fleischer, Nature Phys. **3**, 46 (2007).
[2] B. L. Holian, H. Flaschka, and D. W. Mclaughlin, Phys. Rev. A **24**, 2595 (1981).
[3] P. Poggi, S. Ruffo, and H. Kantz, Phys. Rev. E **52**, 307 (1995).
[4] V. V. Konotop and M. Salerno, Phys. Rev. E **56**, 3611 (1997).
[5] B. L. Holian and G. K. Straub, Phys. Rev. B **18**, 1593 (1978).
[6] V. F. Nesterenko, J. Appl. Mech. Tech. Phys. **24**, 733 (1983).
[7] M. Kameda and Y. Matsumoto, Phys. Fluids **8**, 322 (1996).
[8] M. R. Amin, G. E. Morfill, and P. K. Shukla, Phys. Plasmas **5**, 2578 (1998).
[9] M. Segev, G. C. Valley, and B. Crosignani *et al.*, Phys. Rev. Lett. **73**, 3211 (1994).
[10] D. N. Christodoulides and M. I. Carvalho, J. Opt. Soc. Am. B **12**, 1628 (1995).
[11] J. W. Fleischer, G. Bartal, and O. Cohen *et al.*, Opt. Express **13**, 1780 (2005).
[12] E. Madelung, Zeitschrift fur Physik **40**, 322 (1927).
[13] V. I. Karpman, *Nonlinear Waves in Dispersive Media* (Pergamon Press, New York, 1974).
[14] M. A. Hoefer, M. J. Ablowitz, and I. Coddington *et al.*, Phys. Rev. A **74**, 023623 (2006).
[15] N. K. Efremidis, S. Sears, and D. N. Christodoulides *et al.*, Phys. Rev. E **66**, 046602 (2002).
[16] J. W. Fleischer, T. Carmon, and M. Segev *et al.*, Phys. Rev. Lett. **90**, 023902 (2003).
[17] H. S. Eisenberg, Y. Silberberg, and R. Morandotti *et al.*, Phys. Rev. Lett. **85**, 1863 (2000).
[18] H. S. Eisenberg, Y. Silberberg, and R. Morandotti *et al.*, Phys. Rev. Lett. **81**, 3383 (1998).
[19] D. Mandelik, H. S. Eisenberg, and Y. Silberberg *et al.*, Phys. Rev. Lett. **90** 053902 (2003).
[20] A. V. Gurevich and A. L. Krylov, Zh. Eksp. Teor. Fiz. **92**, 1684 (1987) [Sov. Phys. JETP **65**, 944 (1987)].
[21] A. M. Zheltikov, Phys. Usp. **49**, 605 (2006).
[22] A. V. Gorbach, D. V. Skryabin, and J. M. Stone *et al.*, Opt. Express **14**, 9854 (2006).
[23] P. S. Westbrook, J. W. Nicholson, and K. S. Feder *et al.*, Appl. Phys. Lett. **85**, 4600 (2004).